Automatic 3D US Brain Ventricle Segmentation in Pre-Term Neonates Using Multi-phase Geodesic Level-Sets with Shape Prior

Wu Qiu[1,⋆], Jing Yuan[1,⋆], Jessica Kishimoto[1], Yimin Chen[2], Martin Rajchl[3], Eranga Ukwatta[4], Sandrine de Ribaupierre[5], and Aaron Fenster[1]

[1] Robarts Research Institute, University of Western Ontario, London, ON, CA
[2] Department of Electronic Engineering, City University of Hong Kong, CN
[3] Department of Computing, Imperial College London, London, UK
[4] Sunnybrook Health Sciences Centre, Toronto, CA,
Department of Biomedical Engineering, Johns Hopkins University, MD, USA
[5] Neurosurgery, Department of Clinical Neurological Sciences,
University of Western Ontario, London, ON, CA

Abstract. Pre-term neonates born with a low birth weight ($< 1500g$) are at increased risk for developing intraventricular hemorrhage (IVH). 3D ultrasound (US) imaging has been used to quantitatively monitor the ventricular volume in IVH neonates, instead of typical 2D US used clinically, which relies on linear measurements from a single slice and visually estimates to determine ventricular dilation. To translate 3D US imaging into clinical setting, an accurate segmentation algorithm would be desirable to automatically extract the ventricular system from 3D US images. In this paper, we propose an automatic multi-region segmentation approach for delineating lateral ventricles of pre-term neonates from 3D US images, which makes use of multi-phase geodesic level-sets (MP-GLS) segmentation technique via a variational region competition principle and a spatial shape prior derived from pre-segmented atlases. Experimental results using 15 IVH patient images show that the proposed GPU-implemented approach is accurate in terms of the Dice similarity coefficient (DSC), the mean absolute surface distance (MAD), and maximum absolute surface distance (MAXD). To the best of our knowledge, this paper reports the first study on automatic segmentation of ventricular system of premature neonatal brains from 3D US images.

Keywords: 3D ultrasound, pre-term neonatal ventricle segmentation, multi-phase geodesic level-sets, shape prior, convex optimization.

1 Introduction

Pre-term neonates born with a low birth weight ($< 1500g$) are at increased risk of intraventricular hemorrhage (IVH). The blood within the ventricles and surrounding brain can cause an abnormal accumulation of cerebral spinal fluid

⋆ Contributed equally.

N. Navab et al. (Eds.): MICCAI 2015, Part III, LNCS 9351, pp. 89–96, 2015.
DOI: 10.1007/978-3-319-24574-4_11

(CSF), a condition is called post hemorrhagic ventricle dilatation (PHVD). The progressive dilatation of the ventricles will then cause raised increased intracranial pressure (ICP), leading to potential neurological damage, such as cerebral palsy and neurodevelopmental delay [1]. Trans-fontanel 2D cranial ultrasound (US) is routinely used to monitor any patient born $< 1500g$. Even though IVH is relatively easy to detect using 2D US, it is difficult to assess the progression of ventricle dilatation over time from 2D US planes due to the high user dependency. Clinically, the ventricular size is often estimated qualitatively with 2D US. Because of this inaccurate method of measurement, there is no clinical consensus as to when to perform an interventional therapy (such as a ventricle tap) and how much CSF should be drained [2]. 3D US can be used to quantitatively monitor the ventricular volume in neonates [3,4], and can be done at the bedside. However, to incorporate 3D US into clinical setting, an accurate and efficient segmentation algorithm is highly desirable to extract the ventricular system from the 3D US images.

Previous cerebral ventricle segmentation algorithms have been used extensively for CT [5] and MR images [6], but mainly for adult populations. There are a few studies focusing on neonatal ventricle segmentation [7,8], however, most of them dealt with healthy neonatal MR images. Unlike healthy neonatal MR images, the segmentation of 3D IVH neonate US images poses many more unique challenges, such as US image speckle, low soft tissue contrast, fewer image details of structures, and dramatic inter-subject shape deformation [4,9]. While studies have quantified 3D US ventricle volumes in neonates, all have used manual contouring [3] or user-initialized semi-automatic segmentation [9] in lieu of an automatic approach. In particular, we previously proposed a semi-automatic segmentation approach [10], initialized by a single subject-specific atlas based on user-manual-selected anatomic landmarks. Then, a single-phase level set image segmentation method was used to partition the image into two parts: the background and whole ventricle region. Although a low observer variability was reported in [10], the initial landmark selection was still user dependant, labor intensive and time consuming. Thus, an accurate and efficient automatic ventricle segmentation approach from 3D US images would be required in clinical practice.

Contributions: In this study, we propose an automatic convex optimization based approach for delineating lateral ventricles of pre-term neonates from 3D US images, which makes use of multi-phase geodesic level-sets (MP-GLS) segmentation technique via a variational region competition principle and a spatial prior derived from pre-segmented atlases. In particular, the proposed multi-region segmentation has been parallelized and implemented on a GPU to achieve a speed-up in computation. To the best of our knowledge, this paper reports the first study on automatic segmentation of ventricular system of premature neonatal brains from 3D US images.

2 Method

Segmentation Pipeline: Multiple manually pre-segmented patient images from the training dataset are initially registered to the subject image using affine registration followed by a deformable registration. The multiple registered labels are averaged to acquire a probabilistic labeling map, which serves as a spatial prior for a subsequent segmentation procedure. A thresholding procedure of the probabilistic labeling map follows to generate the initial guess and to approximate intensity appearance model (*i.e.*, the probability density function (PDF)) for each individual sub-region: the left, right ventricle, and background regions respectively. Finally, a MP-GLS based multi-region contour evolution approach is proposed to minimize an introduced energy function, which incorporates the information including the shape prior, the constraints to avoid intersections among structures, the image intensity model, as well as a gradient edge map.

Construction of Spatial Priors: Each training image of $(I_i(x),\, i = 1, 2, ..., n)$ is registered by $\mathbf{u}_i^{affine}(x)$ to the subject image $I_s(x)$ using an affine block-matching approach with default parameters, which is implemented in the Nifty Reg package [11]. Following the affine registration, a recently developed deformable registration algorithm (RANCOR) [12] is used to non-linearly register each pre-segmented image I_i to the subject image I_s by $\mathbf{u}_i^{non-linear}(x)$, $i = 1, 2, ..., n$. Let $L(x) \in \{0, 1, 2\}\ i = 1, 2, ..., n$, be the label function of each pre-segmented image $I_i(x)$, where $\{0, 1, 2\}$ denotes {background, left, right ventricle}. For the simplicity, the average of each label $L(x)$ is used as the probabilistic label function $P_L(x)$, which is used as a probabilistic shape prior and provides a global shape-associated energy cost term in the applied multi-region segmentation. Thresholding $P_L(x)$ using a value of 0.8 generates a binary label image for each sub-region, which provides a proper initial guess to the ventricle segmentation agreed by all the training images. The completely consensus of all the training images is not used in case of an empty set of the intersections of all deformed labels. Therefore, the voxels labeled by this binary image are sampled to approximate the intensity PDF prior $F_L(I(x))$ for each ventricle sub-region.

MP-GLS Segmentation with Spatial Priors: We study the evolution of multiple mean-curvature-driven contours with respect to a disjoint region constraint, for which we propose a novel variational principle, *i.e.*, the *variational region competition*. The proposed *variational region competition* generalizes recent developments in level-set methods and establishes a variational basis for simultaneously propagating multiple disjoint level-sets by means of minimizing costs w.r.t. region changes. In addition, the proposed principle can be reformulated as a spatially continuous Potts problem [13], *i.e.*, a continuous multi-region min-cut problem, which can be solved via convex relaxation under a continuous max-flow perspective [14].

We consider the evolution of n disjoint regions/geodesic level-sets $\mathcal{C}_i$, $i = 1 \ldots n$, under the constraint:

$$\Omega = \cup_{i=1}^{n} \mathcal{C}_i\,, \quad \mathcal{C}_k \cap \mathcal{C}_l = \emptyset\,, \quad \forall k \neq l\,. \tag{1}$$

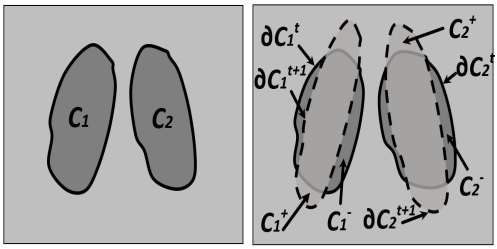

(a) (b)

Fig. 1. An example of the evolution of 2 disjoint regions.(a) 2 disjoint regions at the current time frame t; (b) evolution of two contours from discrete time t to $t+1$, where $\mathcal{C}^{t+1}$ is the evoluted contour at the time frame $t+1$, and $\mathcal{C}^+$ and $\mathcal{C}^-$ show region expansion and shrinkage, respectively.

Let $\mathcal{C}_i^t$, $i = 1 \dots n$, be the i-th region at the current time frame t, which moves to position $\mathcal{C}_i^{t+1}$ at the next time frame $t+1$. For each region $\mathcal{C}_i^t$, $i = 1 \dots n$, at time t, we define two types of difference regions with respect to $\mathcal{C}_i^{t+1}$ (see Fig.1 for an illustration):

1. $\mathcal{C}_i^+$ indicates expansion of $\mathcal{C}_i^t$ w.r.t. $\mathcal{C}_i^{t+1}$: for $\forall x \in \mathcal{C}_i^+$, it is outside $\mathcal{C}_i^t$ at time t, but inside $\mathcal{C}_i^{t+1}$ at $t+1$; for such an expansion, x is assinged with a cost $c_i^+(x)$.
2. $\mathcal{C}_i^-$ indicates shrinkage of $\mathcal{C}_i^t$ w.r.t. $\mathcal{C}_i^{t+1}$: for $\forall x \in \mathcal{C}_i^-$, it is inside $\mathcal{C}_i^t$ at time t, but outside $\mathcal{C}_i^{t+1}$ at $t+1$; for such a shrinkage, x is assinged with a cost $c_i^-(x)$.

With these definitions, we propose the variational principle as: Given n disjoint regions $\mathcal{C}_i$, $i = 1 \dots n$, the evolution of each region over the discrete time frame from t to $t+1$ minimizes total cost of region changes. That is, the new *optimal* contours $\mathcal{C}_i^{t+1}$, $i = 1 \dots n$, minimize the energy:

$$\min_{\mathcal{C}_i} \sum_{i=1}^{n} \Big\{ \int_{\mathcal{C}_i^-} c_i^-(x)\, dx + \int_{\mathcal{C}_i^+} c_i^+(x)\, dx \Big\} + \sum_{i=1}^{n} \int_{\partial \mathcal{C}_i} g(s)\, ds \tag{2}$$

subject to (1), where $g(s)$ is the weighting function along the contour boundaries.

For the mean-curvature-driven evolution of multiple disjoint level-sets $\mathcal{C}_i$, $i = 1 \dots n$, we define the cost functions $c_i^-(x)$ and $c_i^+(x)$, $i = 1 \dots n$, to be proportional to the geodesic distance function from x to the current boundary $\partial \mathcal{C}_i^t$ such that $c_i^-(x) = c_i^+(x) = \text{gdist}(x, \partial \mathcal{C}_i^t)/h\,, \quad i = 1 \dots n$. Using the *variational region competition* principle (2), we have: The mean-curvature-driven evolution of multiple disjoint level-sets $\mathcal{C}_i$, $i = 1 \dots n$, during time frame t to $t+1$ minimizes the cost w.r.t. region changes. The optimal new regions $\mathcal{C}_i^{t+1}$, $i = 1 \dots n$, therefore minimize:

$$\min_{\mathcal{C}_i} \sum_{i=1}^{n} \int_{\mathcal{C}_i \triangle \mathcal{C}_i^t} \frac{1}{h} \text{gdist}(x, \partial \mathcal{C}_i^t)\, dx + \sum_{i=1}^{n} \int_{\partial \mathcal{C}_i} ds \tag{3}$$

subject to the constraint (1), where $\mathcal{C}_t \triangle \mathcal{C}_{t+h}$ denotes the symmetric difference between $\mathcal{C}_t$ and $\mathcal{C}_{t+h}$. For multi-region segmentation in this study, the level-set evolution is driven not only by the geodesic distance functions as above, but also by image features. In general, the cost functions $c_i^-(x)$ and $c_i^+(x)$, $i = 1 \dots n$, w.r.t. region changes are given by the combination of the image feature costs and the geodesic distance functions. In this application, we define the cost functions as follows:

$$c_i^+(x) = c_i^-(x) = -\omega_1 \log F_L(I(x)) - \omega_2 \log \big(P_L(x) * G_\sigma(x)\big) + \omega_3 \frac{1}{h} \operatorname{gdist}(x, \partial \mathcal{C}_i^t) \quad \forall x \in \mathcal{C}_i^t$$

where the weighting parameters $\omega_1, \omega_2, \omega_3 > 0$, $\omega_1 + \omega_2 + \omega_3 = 1$ weight the contributions from the intensity, shape priors and geodesic distance for each voxel, respectively, and $G_\sigma(x)$ is the Gaussian smoothing function. $\omega_1 = 0.3, \omega_2 = 0.4, \omega_3 = 0.3$ were used in our experiments. The corresponding optimization formulation is then given by the *variational region competition* principle (2) directly. We show that the variational problem (2) introduced by the *variational region competition* principle can be equally reformulated as the Potts problem [13]. For this purpose, we define two cost functions $D_i^s(x)$ and $D_i^t(x)$ w.r.t. the current contour $\mathcal{C}_i^t$, $i = 1 \dots n$, at time t:

$$D_i^s(x) := \begin{cases} c_i^-(x)\,, & \text{where } x \in \mathcal{C}_i^t \\ 0\,, & \text{otherwise} \end{cases} \tag{4}$$

$$D_i^t(x) := \begin{cases} c_i^+(x)\,, & \text{where } x \notin \mathcal{C}_i^t \\ 0\,, & \text{otherwise} \end{cases} . \tag{5}$$

Let $u_i(x) \in \{0, 1\}$, $i = 1 \dots n$, be the indicator function of the region $\mathcal{C}_i$. Therefore, the disjoint constraint in (1) can be represented by $\sum_{i=1}^n u_i(x) = 1$; $u_i(x) \in \{0, 1\}\,, \quad \forall x \in \Omega$. Via the cost functions (4) and (5), we can prove that the variational formulation (2) associated with the *variational region competition* principle can be expressed as the Potts problem:

$$\min_{u_i(x) \in \{0,1\}} \sum_{i=1}^n \left\langle u_i, D_i^t - D_i^s \right\rangle + \sum_{i=1}^n \int_\Omega g(x) \left|\nabla u_i\right| \, dx \tag{6}$$

subject to the contour disjointness constraint (1), where the weighted length term in (2) is encoded by the weighted total-variation functions. The resulting formulation (6) gives rise to a challenging combinatorial optimization problem. From recent developments of convex optimization, its global optimum can be approximated efficiently through convex relaxation [15,16].

3 Experiments and Results

Image Acquisition: A motorized 3D US system developed for cranial US scanning of pre-term neonates was used to acquire the images [4]. Following the routine cranial US exam, the 2D US transducer (Phillips C8-5 broadband curved

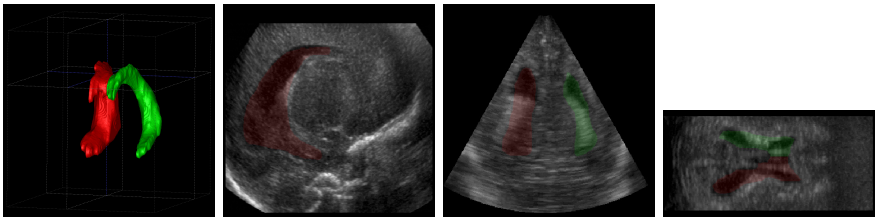

(a) (b) (c) (d)

Fig. 2. An example of segmented ventricles. (a) segmented surface, (b) sagittal, (c) coronal, and (d) transverse views

.

array) was placed into the motorized housing and the 3D US image was acquired. The acquired 3D US image sizes ranged from $300 \times 300 \times 300$ to $450 \times 450 \times 450$ voxels at the same voxel spacing of $0.22 \times 0.22 \times 0.22\, mm^3$. Fifteen patient (with the gestation from 37 to 42 weeks) with different IVH grades were involved in this study. The proposed segmentation approach was evaluated with the 15 patient images using leave-one-out cross validation strategy.

Evaluation Metrics: The proposed segmentation approach was evaluated by comparing the algorithm to manual segmentation results using the Dice similarity coefficient (DSC), the mean absolute surface distance (MAD), and maximum absolute surface distance (MAXD) [17,18].

Results: Figure. 2 shows one example of the algorithm segmented lateral ventricles from an IVH neonate. Quantitative results for the 15 patient images were demonstrated in Table. 1. The proposed approach was implemented using parallel computing architecture (CUDA, NVIDIA Corp., Santa Clara, CA) and the user interface in Matlab (Natick, MA). The experiments were conducted on a Windows desktop with an Intel i7-2600 CPU (3.4 GHz) and a GPU of NVIDIA Geforce 5800X. The mean run time of three repeated segmentations for each 3D US image was considered as the segmentation time to assess the algorithm's efficiency. Each computation of convex optimization required approximately 2 minutes, and each pairwise registration from one training image to the target subject was composed of an affine registration (no GPU acceleration: 3 minutes) and deformable registration (GPU: 50 seconds). Thus, an average of 54 minutes was required for each subject image.

Table 1. Segmentation results of fifteen 3D US images in terms of DSC, MAD, and MAXD, represneted as mean ± standard deviation.

	DSC (%)	MAD (mm)	MAXD (mm)
Left ventricle	72.5 ± 2.8	0.67 ± 0.2	4.1 ± 1.3
Right ventricle	74.0 ± 3.3	0.63 ± 0.3	3.5 ± 1.6
In all	73.2 ± 3.0	0.64 ± 0.3	3.8 ± 1.5

4 Discussion and Conclusion

This paper proposes a GPU-implemented automatic multi-region segmentation approach to extract the lateral ventricles of pre-term neonates from 3D US images, which formulates a MP-GLS segmentation technique via variational region competition, in combination with a spatial prior obtained from pre-segmented atlases. The experimental results using 15 IVH patient images show that the proposed method is accurate and efficient in terms of metrics of DSC, MAD, and MAXD. There were only a few previous studies focusing on 3D US lateral ventricle segmentation problem [9,10]. The DSC of 73.2 ± 3.0 yielded by the proposed approach is higher than the DSC of $72.4 \pm 2.5\%$ reported in [10]. Although [9] reported a higher DSC of $78.4 \pm 4.4\%$, it required careful initialization to the algorithm, which introduced observer variability. Compared to the semi-automatic methods [9,10], the proposed segmentation approach is capable of extracting lateral ventricles in a fully automatic fashon, which does not require any user interactions as input, avoiding observer dependency. The proposed MP-GLS segmentation approach is compared with several other methods using the 15 patient images, including STAPLE, majority voting (MV), single classic level set (SLS), single geodesic level set (SGLS), and multi-phase classic level-sets (MLS). The results show that a mean DSC of 65.5% for STAPLE, 58.3% for MV, 67.4% for SLS, 68.5% for SGLS, and 69.7% for MLS were generated, lower than 73.2% obtained by the proposed method.

The computational time required by the proposed method limits this technique for application at the bedside, where clinicians need to know the ventricle volume immediately after the image acquisition is finished. However, as an off-line processing technique, the proposed technique may be used for the longitudinal analysis of ventricle changes, which could affect specific white matter bundles, such as in the motor or visual cortex, and could be linked to specific neurological problems often seen in this patient population later in life. Considering the small number of images in the employed database, further evaluation experiments are required to cover the anatomical and pathological variation in data.

Acknowledgments. The authors are grateful for the funding support from the Canadian Institutes of Health Research (CIHR) and Academic Medical Organization of Southwestern Ontario (AMOSO).

References

1. Adams-Chapman, I., Hansen, N.I., Stoll, B.J., Higgins, R., et al.: Neurodevelopmental outcome of extremely low birth weight infants with posthemorrhagic hydrocephalus requiring shunt insertion. Pediatrics 121(5), e1167–e1177 (2008)
2. Klebermass-Schrehof, K., Rona, Z., Waldhör, T., Czaba, C., Beke, A., Weninger, M., Olischar, M.: Can neurophysiological assessment improve timing of intervention in posthaemorrhagic ventricular dilatation? Archives of Disease in Childhood-Fetal and Neonatal Edition 98(4), F291–F297 (2013)

3. McLean, G., Coombs, P., Sehgal, A., Paul, E., Zamani, L., Gilbertson, T., Ptasznik, R.: Measurement of the lateral ventricles in the neonatal head: Comparison of 2-d and 3-d techniques. Ultrasound in Medicine & Biology (2012)
4. Kishimoto, J., de Ribaupierre, S., Lee, D., Mehta, R., St Lawrence, K., Fenster, A.: 3D ultrasound system to investigate intraventricular hemorrhage in preterm neonates. Physics in Medicine and Biology 58(21), 7513 (2013)
5. Liu, J., Huang, S., Ihar, V., Ambrosius, W., Lee, L.C., Nowinski, W.L.: Automatic model-guided segmentation of the human brain ventricular system from CT images. Academic Radiology 17(6), 718–726 (2010)
6. Liu, J., Huang, S., Nowinski, W.L.: Automatic segmentation of the human brain ventricles from MR images by knowledge-based region growing and trimming. Neuroinformatics 7(2), 131–146 (2009)
7. Wang, L., Shi, F., Lin, W., Gilmore, J.H., Shen, D.: Automatic segmentation of neonatal images using convex optimization and coupled level sets. NeuroImage 58(3), 805–817 (2011)
8. Shi, F., Fan, Y., Tang, S., Gilmore, J.H., Lin, W., Shen, D.: Neonatal brain image segmentation in longitudinal MRI studies. NeuroImage 49(1), 391–400 (2010)
9. Qiu, W., Yuan, J., Kishimoto, J., McLeod, J., de Ribaupierre, S., Fenster, A.: User-guided segmentation of preterm neonate ventricular system from 3d ultrasound images using convex optimization. Ultrasound in Medicine & Biology 41(2), 542–556 (2015)
10. Qiu, W., Yuan, J., Kishimoto, J., Ukwatta, E., Fenster, A.: Lateral ventricle segmentation of 3D pre-term neonates US using convex optimization. In: Mori, K., Sakuma, I., Sato, Y., Barillot, C., Navab, N. (eds.) MICCAI 2013, Part III. LNCS, vol. 8151, pp. 559–566. Springer, Heidelberg (2013)
11. Ourselin, S., Stefanescu, R., Pennec, X.: Robust registration of multi-modal images: towards real-time clinical applications. In: Dohi, T., Kikinis, R. (eds.) MICCAI 2002, Part II. LNCS, vol. 2489, pp. 140–147. Springer, Heidelberg (2002)
12. Rajchl, M., Baxter, J.S., Qiu, W., Khan, A.R., Fenster, A., Peters, T.M., Yuan, J.: Rancor: Non-linear image registration with total variation regularization. arXiv preprint arXiv:1404.2571 (2014)
13. Potts, R.B.: Some generalized order-disorder transformations. Proceedings of the Cambridge Philosophical Society 48, 106–109 (1952)
14. Yuan, J., Ukwatta, E., Tai, X.C., Fenster, A., Schnoerr, C.: A fast global optimization-based approach to evolving contours with generic shape prior. Technical report CAM-12-38, UCLA (2012)
15. Yuan, J., Bae, E., Tai, X.-C., Boykov, Y.: A continuous max-flow approach to potts model. In: Daniilidis, K., Maragos, P., Paragios, N. (eds.) ECCV 2010, Part VI. LNCS, vol. 6316, pp. 379–392. Springer, Heidelberg (2010)
16. Lellmann, J., Breitenreicher, D., Schnörr, C.: Fast and exact primal-dual iterations for variational problems in computer vision. In: Daniilidis, K., Maragos, P., Paragios, N. (eds.) ECCV 2010, Part II. LNCS, vol. 6312, pp. 494–505. Springer, Heidelberg (2010)
17. Qiu, W., Yuan, J., Ukwatta, E., Sun, Y., Rajchl, M., Fenster, A.: Dual optimization based prostate zonal segmentation in 3D MR images. Medical Image Analysis 18(4), 660–673 (2014)
18. Qiu, W., Yuan, J., Ukwatta, E., Sun, Y., Rajchl, M., Fenster, A.: Prostate segmentation: An efficient convex optimization approach with axial symmetry using 3D TRUS and MR images. IEEE Trans. Med. Imag. 33(4), 947–960 (2014)